Numerical Evaluation of Cyclone Application for Impurities Removal from Molten Aluminum

A.N. TURCHIN, D.G. ESKIN, and L. KATGERMAN

The purification of gaseous and liquid media by means of a cyclone concept is well known and has been successfully applied in different industries. While the impurities removal from molten metal has been an important issue for many years, to the best of our knowledge, the application of a cyclone concept has rarely been considered for molten metal applications. The presence of impurities in cast products is detrimental to their quality. In this article, computer simulations are used to evaluate the possibilities of cyclone application in molten aluminum processing by determining the following: the fluid flow for flow velocities of 0.01, 0.1, and 1 m/s; the particle behavior for discrete particle sizes in the range of 20 to 100 μm; and the collection efficiency of the cyclone. The geometrical features are discussed. The results show that the cyclone concept can be effectively used as an alternative method to remove the impurities from a stream of molten aluminum in a wide range of flow regimes.

DOI: 10.1007/s11663-008-9127-9

I. INTRODUCTION

A cyclone separator is one of the most popular units in the industrial practice of separation or removal of impurities from a gas or liquid. The advantages of the cyclone that make it attractive for industrial application include the absence of moving parts, low operational costs, and design simplicity.

Impurities in casting practice are always a crucial issue determining the quality of cast products. Entrapped oxides in the form of films and particles are the most common incidents in the solidified metal.[1] The level of oxides and inclusions in the molten metal in today's cast house is controlled by filter boxes[2] and degassing units.[3,4] However, the application of such systems, *i.e.*, filter boxes, can be limited. During the transfer of molten metal through these systems, the pick up of earlier removed impurities occurs, leading to the varying efficiency of the filter (*i.e.*, filter aging).[5] Moreover, expensive filters have to be replaced regularly. While the impurities removal from molten metal has remained the important issue for many years, to the best of our knowledge, the application of a cyclone for molten metal processing has rarely been considered until recently.[6,7] The removal of entrained in the molten steel low density particles (alumina) in a cyclone with an axial, cylindrical capture surface has been studied numerically, using commercially available software with incorporated turbulence models by Slack and Wraith.[6] By assuming particle adhesion to the solid core, optimizing the design of the cyclone, and applying the process conditions corresponding to the practical scale, they demonstrated using the Reynolds stress model (RSM) that all particles larger in size than 35 μm and a considerable portion of those between 15 and 30 μm were removed from the stream of molten steel. Later, Zuidema adapted a more conventional cyclone design for alumina removal from the stream of molten aluminum.[7] A series of calculations using the renormalized group model (RNG, $k - \varepsilon$) aimed at the efficiency of the cyclone resulted in a patent.[8] However, the results of this work were obtained only for a fixed inlet velocity of 0.01 m/s, which is far less than those commonly occurring in a cast house.

In spite of the fact that the operation of hydrocyclones acting mostly with an air core has been sufficiently understood and improved owing to the development of computational fluid dynamics and recent advances in computational power, many questions still remain answered in regards to transferring the cyclone concept to molten metal processing. What are the consequences of operating the cyclone without free surface or air core? In particular, how does the flow pattern in the cyclone operating with the molten aluminum on an industrial scale affect the behavior of impurities with density close to that of the fluid, and what is the cyclone performance for discrete particles? What is the cyclone efficiency in the range of inlet velocities from 0.01 to 1 m/s? What is the height of molten metal at the inlet required to provide a metallostatic pressure driving the melt through the cyclone?

In this article, the numerical simulations of fluid and particle flows are presented for the following two types of cyclones: the first using the dimensions proposed by Zuidema;[7] and the second using a container for impurity deposition. The cyclones are applied for impurities removal from the stream of molten

A.N. TURCHIN, PhD Student, and D.G. ESKIN, Senior Scientist, are with the Netherlands Institute for Metals Research, 2628CD Delft, The Netherlands. L. KATGERMAN, Professor, is with the Department of Materials Science and Engineering, Delft University of Technology, 2628CD Delft, The Netherlands. Contact e-mail: a.turchin@nimr.nl. Contact e-mail: a.turchin@nimr.nl

Manuscript submitted July 11, 2007.
Article published online February 20, 2008.

aluminum. The article is organized as follows: we start with engineering aspects for cyclone application in molten metal processing and general concept description in Section II; the validation of the code used to model the cyclone performance operating with molten aluminum is presented in Section III; the formulation of the problem with specific assumptions, the equations comprising the model used, and general computational procedures are described in Section IV; the results and discussion are highlighted in Section V; and finally, Section VI is devoted to conclusions. A nomenclature of symbols is given at the end of the article.

II. DEVICE AND CONCEPT DESCRIPTION

The geometrical model and schematic drawing with variable parameters of the cyclone proposed for impurities removal from the molten aluminum alloy are shown in Figures 1(a) and (b). The axis (1) is parallel to the gravity direction. The device consists of a block of ceramic material (2) in which a conical chamber (3) has been made. An inlet (4) into the chamber (3) has either a rectangular or round section and is tangential to the cone. Above the inlet, there is an outlet pipe (5). At the bottom of the conical chamber (3), there is a cylindrical container for impurities deposition indicated by (6) and

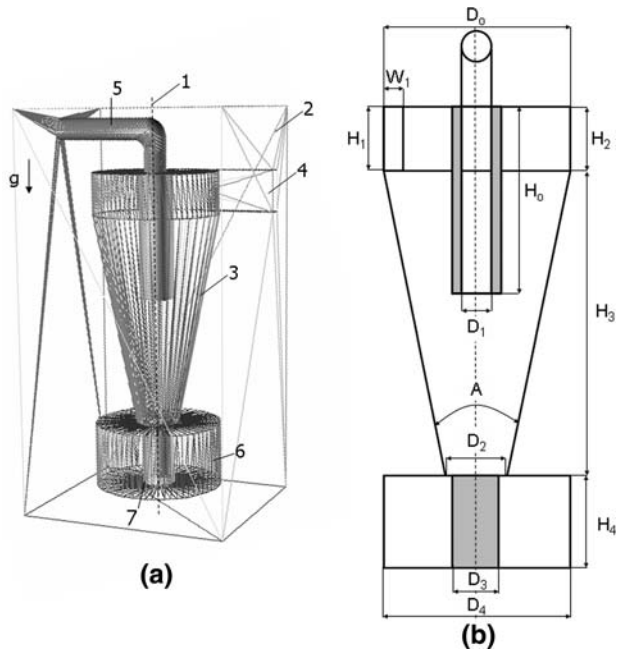

Fig. 1—Geometrical model (*a*) (1—vertical axis, 2—ceramic block, 3—conical chamber, 4—inlet, 5—outlet, 6—container for impurities deposition, and 7—core) and schematic drawing (*b*) of the cyclone (W_1—width of the inlet window, H_0—length of the "vortex finder," H_1—height of the inlet window, H_2—height of the cylindrical part of the chamber, H_3—height of the conical part of the chamber, H_4—height of the container for impurities deposition, D_0—diameter of the cylindrical part of the chamber, D_1—diameter of the outlet pipe, D_2—diameter of the bottom part of the conical chamber, D_3—diameter of the core in container for impurities deposition, D_4—diameter of the container for impurities deposition, and A—cone angle).

a built-in core (7) with the height equal to the height of the container. At this point, it is worth mentioning that the container with the core is a design feature introduced in the present work, as compared with the initial design proposed by Zuidema.[7] When molten aluminum is poured in the inlet (4), it enters the conical chamber (3). Due to tangential introduction of the molten metal, an adequate degree of the spiral motion is initiated downward in the chamber (3) around the axis (1). In such a way, impurities are deposited through the space between the core (7) and wall of the conical chamber (3) in the container (6). The flow reverses from the bottom wall of the core and is transferred into a stable, vertical flow directed into the outlet pipe (5). Table I lists the variable geometrical parameters that are used in this study.

The cyclone used for impurities removal from the stream of molten aluminum presented in Figure 1 works by initiation of the spiral motion in the "dirty" melt and, therefore, by producing increased radial acceleration on impurities. These are oxide particles and films generated by surface disturbances in the metal flow with free surfaces and ceramic inclusions due to the melt transfer from the furnace through the metal distribution system. The density of suspended impurities is usually only 10 to 60 pct more than the density of molten aluminum. Tangential inflow of the melt results in a stronger force acting on a larger particle with a higher density, pushing it helically downward. Smaller particles can be easily captured by the outgoing melt flow.[9] Looking at this phenomenon occurring in molten aluminum processing from a different prospective, capturing of small particles by outflow is not considered to be a problem. Since the grain refinement treatment (*i.e.*, by AlTiB) is a common practice in aluminum casting, the removal of small particles ($d_p \leq 20$ μm) becomes even undesirable. Furthermore, 20 μm is the minimum inclusion size that can be detected by available techniques, *i.e.*, liquid metal cleanliness analyzer (LIMCA).[10]

While the principal mechanism of impurities separation from the liquid media is similar to a conventional hydrocyclone, the design and operation of the cyclone presented in Figure 1 differs significantly. The continuously operating conventional hydrocyclone has two outlets centered at the axis of the cyclone. Thus, during operation the particles are permanently leaving the hydrocyclone with the underflow, while the purified liquid moves upward. The hydrocyclone usually operates with the top open to the atmosphere, promoting the formation of the air core due to the low pressure at the cyclone axis. Extreme inlet velocities (> 5 m/s) contribute to air core formation.[11] Additionally, two outlets and high inlet velocities result in a high pressure drop through the cyclone.[12] The application of a cyclone to molten-aluminum processing obviously requires only one outlet and the prevention of free surfaces formation. Taking into account that the conventional aluminum casting processes, such as direct-chill casting, *etc.*, are usually semicontinuous, it was decided to have one outlet and to include the container for impurities deposition to the earlier proposed design.[6] When the casting process is finished and the cleaning of the cyclone from impurities is required, the dirty metal can

Table I. Dimensions of Cyclones Considered in the Present Study

Cyclone Type	Dimension as Indicated in Figure 1(b) (m)											
	*W*1	*Ho*	*H*1	*H*2	*H*3	*H*4	*D*0	*D*1	*D*2	*D*3	*D*4	$A^{\dagger}$
1*	0.03	0.3	0.1	0.1	0.5	—	0.3	0.05	0.1	—	—	25
2**	0.03	0.3	0.1	0.1	0.5	0.15	0.3	0.05	0.1	0.075	0.3	25

*Cyclone according to Zuidema.[7]
**With container attached.
†*A* in deg.

be extracted thought the opening in the bottom part of the cyclone. The phenomenon of air core may cause additional problems, such as enhanced entrapment of oxide films from the free surface, *etc*., and, therefore, should be avoided. The flow velocities through melt-guiding systems in casting practice are considered to be not more than 1 m/s. In terms of efficiency, it is well known that a higher inlet velocity or pressure generally results in the increased performance of a hydrocyclone, since the removal of the particles with underflow can be significantly intensified.[13] The present design is aimed at the collection of the impurities in the body of the cyclone and, therefore, bringing us to the question of how will it affect the efficiency.

III. FORMULATION OF THE PROBLEM

The multiphase flow problem for the cyclone can be solved by consistent treatment of each phase. In this article, we considered a cyclone operating at a constant inlet velocity and without internal air core. The cyclone is intended for the removal of impurities from the stream of molten aluminum. Heat transfer between the molten metal and interior surface of the cyclone is neglected, as it is assumed to be made from refractory material. Only spherical particles are considered. Furthermore, it is assumed that due to a relatively low volumetric concentration of the particles (inclusion size in the range 20 to 100 μm), the fluid motion is not affected by the particle motion. Based on the last assumption, a two-step approach common in modeling of two-phase flow problems is implemented. First, the fluid flow equations are solved without considering the particles in the system. Second, as the steady-state solution for the flow in the system is reached, the particle transport calculations are performed in a constant steady-state velocity field.

The governing equations for the velocity field in an incompressible fluid and for the particles affected by fluid motion can be described by the Navier–Stokes equations with some additional terms (Eq. [1]), by a mass continuity equation (Eq. [2]), and by a particle transport equation (Eq. [3]) presented in Table II.[14]

The flow in the conical chamber of a cyclone is typically turbulent. A strong swirl, flow reversal, *etc*., additionally introduces anisotropy and strain into the turbulence. The use of a suitable turbulence model in the numerical calculations of a cyclone is crucial for correct prediction of flow pattern and separation efficiency. Many attempts have been made to investigate turbulence models for the flow pattern in a hydrocyclone. Bhaskar *et al*.[15] have compared the experimental and simulation results generated using different turbulent models, such as $k-\varepsilon$, RNG $k-\varepsilon$, and RSM. In the $k-\varepsilon$ model, it is assumed that turbulence is isotropic and only one scalar-velocity fluctuation is modeled. Due to this assumption, the swirling component of velocity in a hydrocyclone is shown to be unrealistically small, and the $k-\varepsilon$ model provides a solution with an error of approximately 15 to 20 pct. The results obtained with the RNG $k-\varepsilon$ turbulence model[16] indicate a

Table II. Main Equations Comprising the Model Used[14]

Navier–Stokes equation	$\frac{\partial}{dt}(\rho\mathbf{u}) + \nabla\cdot(\rho\mathbf{uu}) = -\nabla p + \nabla\cdot(\tau) + \rho\mathbf{g} + \mathbf{F}$	[1]
Continuity equation	$\frac{\partial\rho}{dt} + \nabla\cdot(\rho\mathbf{u}) = 0$	[2]
Particle transport for spherical particle	$\frac{\pi}{6}d_p^3\rho_p\frac{\partial\mathbf{u}_p}{dt} = \frac{\pi}{6}d_p^3(\rho_p g - \nabla p) + \frac{1}{2}C_D\frac{\pi}{4}d_p^2\rho(\mathbf{u}-\mathbf{u}_p)\lvert\mathbf{u}-\mathbf{u}_p\rvert$	[3]
Turbulence kinetic energy	$\frac{\partial}{\partial t}(\rho k) + \frac{\partial}{dx_i}(\rho k u_i) = \frac{\partial}{dx_j}\left(\alpha_k\mu_{\text{eff}}\frac{\partial k}{\partial x_j}\right) + P + G - \rho\varepsilon$	[4]
Turbulence dissipation rate	$\frac{\partial}{\partial t}(\rho\varepsilon) + \frac{\partial}{dx_i}(\rho\varepsilon u_i) = \frac{\partial}{dx_j}\left(\alpha_\varepsilon\mu_{\text{eff}}\frac{\partial\varepsilon}{\partial x_j}\right) + c_{\varepsilon 1}\frac{\varepsilon}{k}(P + c_{\varepsilon 3}G) - c_{\varepsilon 2}^*\rho\frac{\varepsilon^2}{k}$	[5]
Supplementary equations for turbulence model	$\mu_{\text{eff}} = \mu + \mu_t$	[6]
	$\mu_t = \rho c_\mu\frac{k^2}{\varepsilon}$	[7]
	$c_{\varepsilon 2}^* = c_{\varepsilon 2} + \frac{c_\mu\rho\eta^3(1-\eta/\eta_0)}{1+\beta\eta^3}$	[8]
	$\eta = S_{ij}\frac{k}{\varepsilon}$	[9]
	$S_{ij} = \frac{1}{2}\left(\frac{\partial u_i}{\partial x_j} + \frac{\partial u_j}{\partial x_i}\right)$	[10]
Supplementary equations for particle transport	$C_D = \frac{24}{\text{Re}_D} + \frac{6}{1+\sqrt{\text{Re}_D}} + 0.4$	[11]
	$\text{Re}_D = \frac{d_p(\mathbf{u}-\mathbf{u}_p)}{\nu}$	[12]

reasonably good prediction for the flow field. Bhaskar *et al.*[15] found for throughput and water split in the cyclone that the simulated results, using the RNG $k-\varepsilon$ model, match with the experimental results with an error of 8 to 15 pct. Due to the fact that the RSM model[17] solves the transport equation for each individual Reynolds stress, it enables one to model anisotropic turbulence and strained flow with a much better precision, namely with an error of 4 to 8 pct,[15] for the swirling flow. Finally, the increased computational power allows one to apply the large eddy simulations for the problems, where large turbulent structures have to be predicted with high accuracy.[18] However, two last models still require significant computational efforts that make them impractical for the three-dimensional (3-D) simulations of cyclone performance.

In the present article, the RNG $k-\varepsilon$ model has been chosen for the simulation of the turbulent flow in the cyclone, being a compromise between the computational time and the accuracy of the results.

The RNG $k-\varepsilon$ model applies statistical methods for derivation of the averaged equations for turbulence quantities, such as turbulent kinetic energy, k (Eq. [4]), and its dissipation rate, ε (Eq. [5]) (Table II). The equations are similar to the equations for the $k-\varepsilon$ model. However, equation constants that are found empirically in the standard $k-\varepsilon$ model are derived explicitly in the RNG $k-\varepsilon$ model.[14]

The turbulence quantities in the RNG $k-\varepsilon$ model implemented in Flow-3D are calculated by the transport Eqs. [6] through [10] shown in Table II. Some additional empirical constants used in Eqs. [4] through [10] are the coefficients $c_\mu = 0.0845$, $c_{\varepsilon 1} = 1.42$, $c_{\varepsilon 2} = 1.68$, $\eta_0 = 4.38$, $\beta = 0.012$, $a_k = 0.72$, and $a_\varepsilon = 0.72$ (Table II).[14]

The particle flow in the cyclone is simulated using the tracking technique where each particle can be treated as an isolated body. When tracking the motion of particles in the cyclone, a Lagrangian frame of reference is employed in order to solve the particle momentum equation (Eq. [3] in Table I).

In the equation of particle motion, inertia is included in the particle mass, represented by the density of the particle material. Buoyancy comes from the combination of the gravity and fluid pressure terms in Eq. [3]. The lift of the particle due to buoyancy is also taken into account, but not due to a nonzero shear.[14]

The effect of turbulence on the particle trajectories can play a major role on particle behavior when the inertia of the particle is small, and it responds to the velocity fluctuations of the continuous phase caused by turbulence. Otherwise, it can be neglected. However, in the calculations presented in this paper the turbulance effect has not been taken into account. Note that particles do not interact with each other.[14]

There are no experimental data available on the interaction between the inclusions in molten aluminum and refractory material in casting practice. This interaction is described in the model using the coefficient of restitution, c, which defines the ratio of the normal components of the particle velocity after and before the impact with a wall. One can expect that either the inclusion will stick to the wall of refractory material or its velocity will be significantly reduced and it will be brought downward by the axial flow, *i.e.*, down to container in a type 2 cyclone. Both scenarios, most probably, will increase the efficiency of the cyclone. However, in order to complicate the simulation, we assumed that there is a loss of particle kinetic energy during reflection, but it is not significant, and therefore, $c = 0.95$.

The simulations were carried out on two types of cyclones with the dimensions given in Table I. A molten Al–4.5 pct Cu alloy is considered, with the physical properties available elsewhere.[19] A Cartesian-coordinate system is used. The turbulence model described previously is included into the code. The governing Navier–Stokes equations are solved in the code for the defined values of convergence, which is 10^{-6} for momentum equations. In this article, the general minimum residual pressure–velocity coupling technique is employed. The equations are discredited by a finite-volume method, using the second-order monotonicity-preserving upwind-difference algorithm. More details on the pressure–velocity coupling algorithm, discretisation scheme, set of equations, and models used can be found elsewhere.[14]

A 3-D domain with a structured uniform mesh with a cell size of 0.007 m includes the conical chamber, inlet with a rectangular cross section, and outlet as a round pipe. The cell size used is required, according to the preliminary parametric study, for a correct solution for the velocity pattern within reasonable computational time without a significant reduction in accuracy of flow pattern and cyclone performance compared with a finer grid. The flow pattern is obtained for the three inlet flow velocities of 0.01, 0.1, and 1 m/s. The fixed pressure boundary conditions are used at the outlet. The inclusions are modeled as discrete mass particles with a size range of 20 to 100 μm and densities in the range of 2660 to 3980 kg/m^3. The density interval covers the following values of density of the inclusions commonly present in molten aluminum: $\rho_{SiO_2} = 2660\,\text{kg/m}^3$, $\rho_{\gamma-Al_2O_3} = 3200\,\text{kg/m}^3$, $\rho_{MgO} = 3580\,\text{kg/m}^3$, $\rho_{Al_2MgO_4} = 3640\,\text{kg/m}^3$, and $\rho_{\alpha-Al_2O_3} = 3980\,\text{kg/m}^3$.[20]

Three series of calculations were performed for the following purposes: (1) to determine the efficiency of the cyclone for discrete particle sizes having an identical density of 3300 kg/m^3; (2) to obtain qualitatively the particle distribution in the cyclone depending on the particle size and density; and (3) to determine the metal head at the inlet necessary for cyclone operation.

For the first series of calculations, the particles were randomly and uniformly generated at the inlet window with the generation rate according to the reference data on typical inclusion size distribution in molten aluminum[20,21] and recalculated for the considered flow velocities (Figure 2). The operation of the cyclone with the injected particles continued until the steady state in the number of particles trapped by the cyclone reached, *i.e.* 10 to 1000 seconds, depending on the flow velocity and number of particles. Finally, the efficiency of the cyclone under different process conditions was obtained as a slope of the function, *i.e.*, particle number trapped by the cyclone *vs* time.

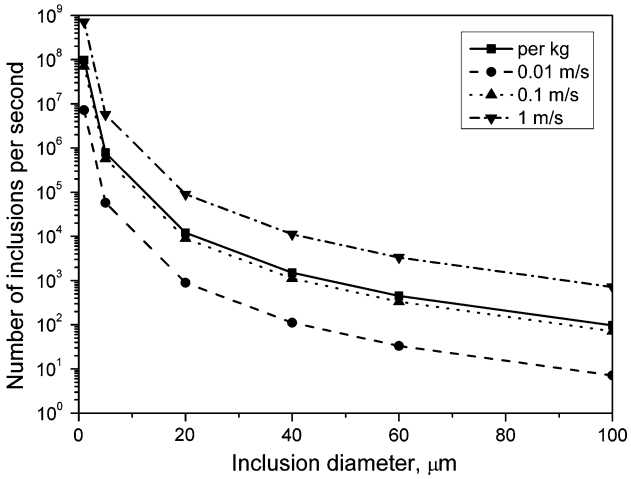

Fig. 2—Experimental data on inclusion size distribution in molten metal per kilogram[20,21] recalculated for the considered inlet flow velocities (0.01, 0.1, and 1 m/s).

For the second series of calculations, the particle distributions for the cyclone (type 2) operating at an inlet velocity of 1 m/s with different particle densities and identical particle size of 20 μm and for different particle sizes of 20 to 100 μm and identical particle density of 3300 kg/m^3 were simulated. The particles entered the cyclone at a rate of 1000 particles per second for each fraction.

For the third series of calculations, to calculate the effect of the metal head on the inlet velocity, a basin of 0.38×0.36 m^2 with a molten Al–4.5 pct Cu alloy was attached to inlet of the type 1 cyclone. The level of molten aluminum was kept constant during the cyclone operation. The fixed pressure boundary conditions were used at the outlet with the value corresponding to the metallostatic pressure equal to 0.1 m of melt. The following heights of molten metal in the basin were used: 0, 0.24, 0.27, 0.30, 0.6, and 0.8 m. The average inlet velocity was then obtained in the transverse plane of the inlet.

IV. BENCHMARK STUDY

Having discussed the cyclone concept and its application for molten aluminum processing, the code to be used in the present work has to be validated. The numerical study of Gupta and Kumar,[22] with a thorough description of computational procedure, was used to verify the RNG $k-\varepsilon$ turbulence model implemented into the commercial software Flow-3D*

*Flow-3D is a trademark of Flow Dynamics Inc., Santa Fe, NM.

(Ver. 9.2). Their article presents results on the dynamics of 3-D water flow in a cyclone obtained using particle tracking velocimetry (PTV) and a 3-D computational model. The cyclone used is a cylinder of an inside axial length of 0.406 m and an inside diameter of 0.203 m,

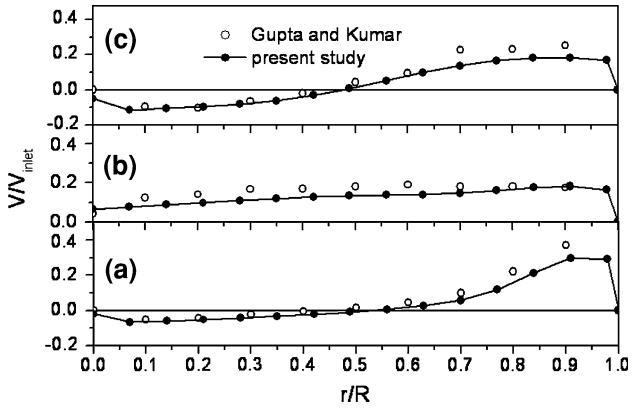

Fig. 3—Tangential velocity profiles for at the cross sections of (*a*) $z/D = 0.094$, (*b*) $z/D = 1$, and (*c*) $z/D = 1.925$ obtained by Gupta and Kumar[22] and using Flow-3D in this work.

with the inlet and outlet tangentially located at the opposite ends of the cylinder and oriented in such a way that the flow helix is right handed. The turbulence model equations and empirical constants in the model of Gupta and Kumar[22] and in Flow-3D used are identical.

In Figures 3(a) through (c), the profiles of mean tangential-velocity components with the same inlet conditions are shown for characteristic positions $z/D = 0.094$, $z/D = 1$, and $z/D = 1.925$, respectively. The results predicted by Flow-3D and the model of Gupta and Kumar are quite similar. An illustrative comparison for tangential velocity at an axial location of $z/D = 0.75$ ($z = 0.152$ m) for Re = 18,000 is shown in Figure 4. As can be seen, while the velocity gradient is well predicted near the top of the cylinder ($\theta = 0$ deg), the velocity profile near the side ($\theta = 90$ deg) obtained numerically is quite far from experimental data. This is probably due to fact that the vortex center is non-stationary, and the numerical model cannot account for this behavior.[22] With taking into account the experimental uncertainty of approximately 15 pct, the numerical results obtained by Gupta and Kumar and using Flow-3D are considered to be in a good agreement with experimental results. Hence, the numerical code used in this study is validated.

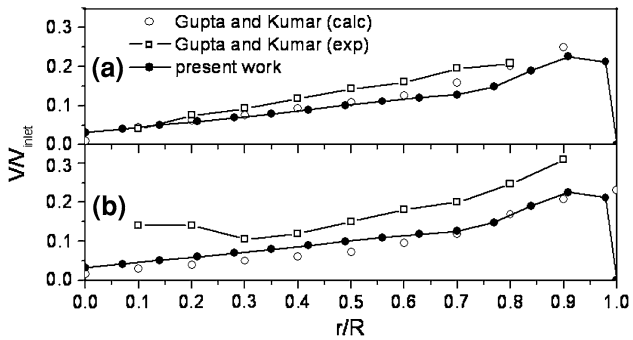

Fig. 4—Tangential velocity profiles for Re = 18,000 at $z/D = 0.75$ for different azimutal angle of (*a*) $\theta = 0$ deg and (*b*) $\theta = 90$ deg obtained by Gupta and Kumar[22] from PTV experiments, computations and using Flow-3D in this work.

V. RESULTS AND DISCUSSION

A. *Flow Pattern*

The axial and tangential velocity contours obtained in radial planes at different heights for both types of the cyclone are presented in Figures 5 and 6, respectively. Note that the dimensionless velocity is given by V/V_{in}. Since the cyclone has only one tangential inlet, the axis of the cyclone does not coincide with the axis of the vortex, and velocity profiles are not symmetric. Two axial flows can be generally distinguished, divided by dotted lines in Figure 5, with the dotted line moving upward indicated by positive velocity; and with the one directed downward indicated by negative velocity. The positive axial velocity decreases outward from the cyclone axis, and at a specific position, it changes to negative. The relatively weak axial flows, both upward and downward, are observed in the container for particle deposition of the type 2 cyclone (Figure 5(b)).

Tangential velocity profiles obtained at different heights in the cyclones are plotted in Figure 6. With an increase in the radial distance from the cyclone axis, the value of the tangential component increases, and after reaching the maximum, it steeply decreases to zero at the wall. For the type 1 cyclone, the profiles remain qualitatively the same, irrespective of the axial height in the cyclone chamber (Figure 6(a)); while for the type 2 cyclone, the profile is shifted off axis at a height of 0.2 m, likely due to the vertically oriented axial flow in this region (Figure 6(b) and 5(b)). The weak tangential flow is also present in the container of the type 2 cyclone (Figure 6(b)). For both types of cyclone, the maximum value of the tangential velocity is observed at the top of the cyclone, and it decreases toward the bottom of the cyclone. It also can be concluded from Figures 5 and 6 that the tangential velocity is the most dominant velocity component in the cyclone.

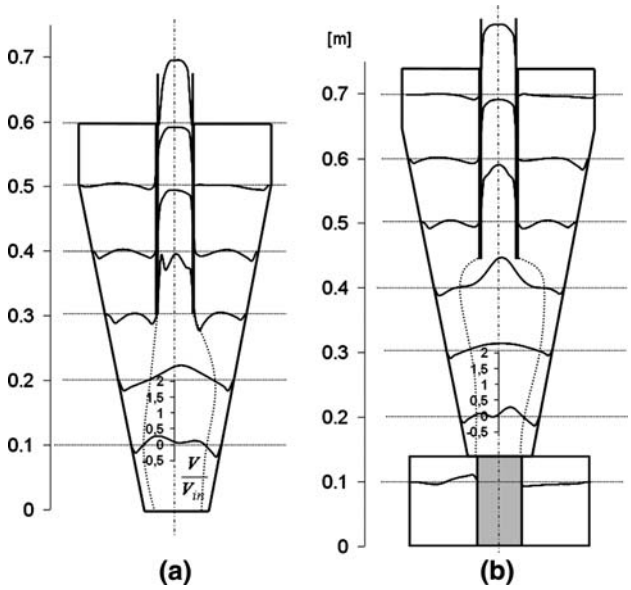

Fig. 5—Axial velocity distributions (dimensionless velocity (V/V_{in})) in molten metal at different vertical positions inside the conical chamber of the cyclone for cyclones of (*a*) type 1 and (*b*) type 2; scale shown for the lowest sections $z = 0.1$ m is applied for all profiles.

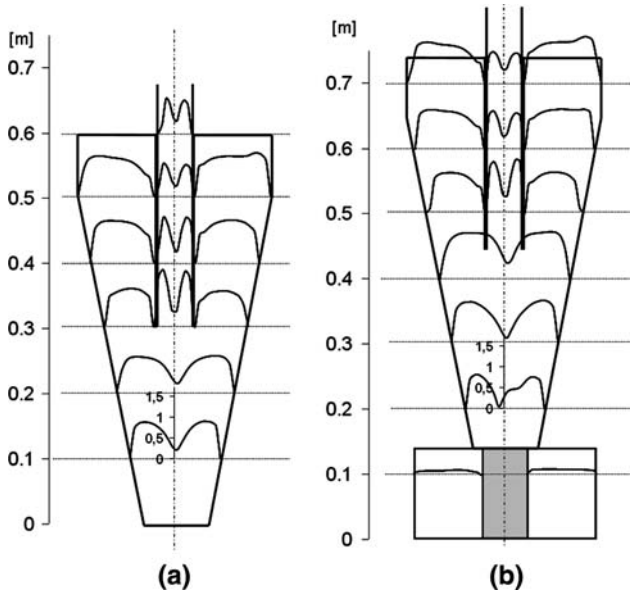

Fig. 6—Tangential velocity distributions (dimensionless velocity (V/V_{in})) of molten metal at different vertical positions inside the conical chamber of the cyclone for cyclones of (*a*) type 1 and (*b*) type 2; scale shown for the lowest sections $z = 0.1$ m is applied for all profiles.

These observations on axial and tangential profiles in the chamber of the cyclone agree qualitatively well the data published earlier.[15]

B. *Particle Behavior*

Figures 7(a) through (e) demonstrate five particle trajectories for both types of cyclone considered in the present article, operating at 0.01 m/s (Figures 7(a) and (b)) and 1 m/s (Figures 7(c) through (e)). Although it is extremely difficult to distinguish separately the effect of different forces in such a complex phenomenon of particle-fluid interaction, some general comments can be made.

Considering the case when the inlet velocity is 0.01 m/s and particle size is 20 μm (Figures 7(a) and (b)), it can be observed that some particles entering the type 1 cyclone move downward helically along the inner wall due to centrifugal force, and when they reach the bottom wall, they can be captured by the vertically oriented axial flow (within the dotted line in Figure 5(a)) and lifted up into the outlet pipe (Figure 7(a)). It is also worth mentioning that for this particular case, a substantial amount of particles remains in the cyclone due to a very small velocity gradient in the molten aluminum. The fact that the particles are denser than the conveying them fluid contributes to particle capture by the cyclone. The presence of the container at the bottom of the type 1 cyclone can improve the entrapment of the particles in the cyclone (Figure 7(b)). The flow in the container is characterized by small axial and tangential

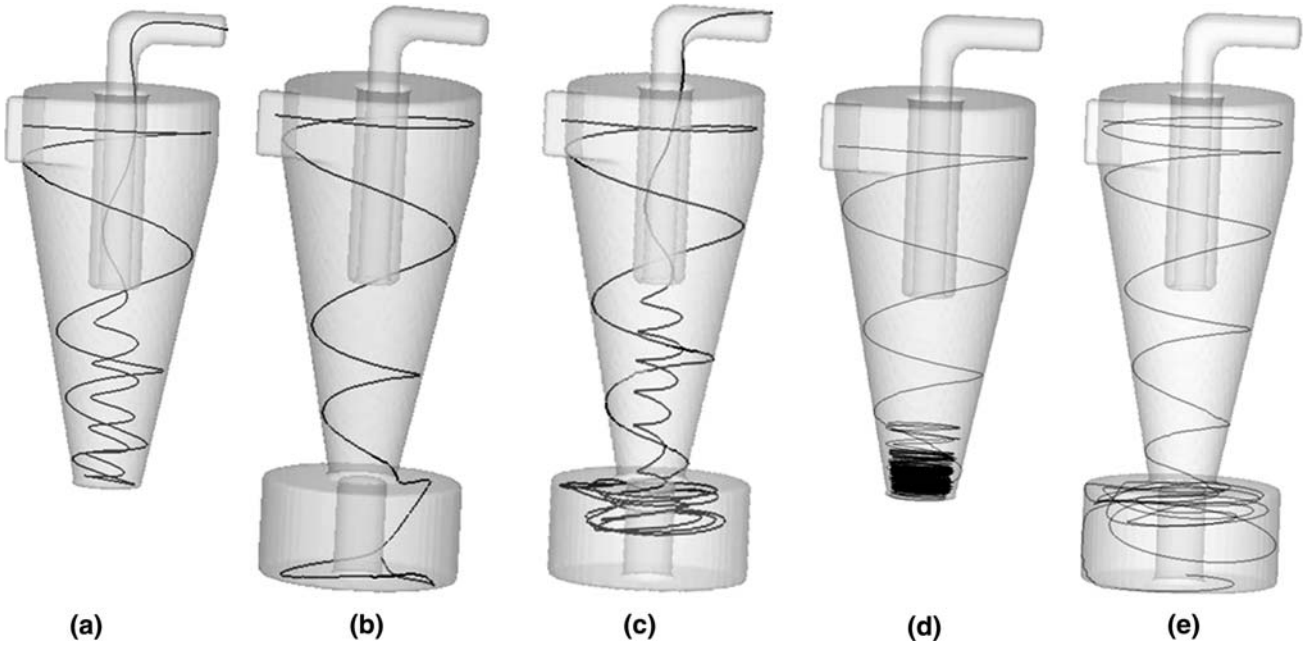

Fig. 7—Particle trajectories in two cyclones of (*a*) and (*d*) type 1 and (*b*), (*c*), and (*e*) type 2, operating with inlet velocities of (a) and (b) 0.01 m/s and (c) through (e) 1 m/s for spherical particles of (a) through (c) 20 μm and (d) and (e) 100 μm.

velocities (Figures 5(b) and 6(b)). Once a particle enters the container, it is rather difficult for it to leave the low-velocity gradient field.

The situation changes as the strong flow at the inlet is applied (Figure 7(c)). The fine particle is brought into the container by the increased tangential flow; however, instead of settling to the bottom of the container, the fine particle rotates around the solid core at the top region of container until it is lifted by the existing upward axial flow (Figure 5(b)).

By comparing the different types of cyclone, the identical inlet velocity of 1 m/s, and the same particle size of 100 μm, one can see that large particles can be effectively captured by the cyclones (Figures 7(d) and (e)). This behavior can be explained by the fact that particles of a larger size experience greater centripetal acceleration, therefore decreasing the chance that the particles will cross the boundary of downward/upward axial flow (dotted line in Figure 5) and increasing the efficiency of the cyclone (Figure 7(d)). The particle comes to rest at the bottom of the cyclone or in the container.

The calculations with different particle densities at the same particle size of 20 μm in the type 2 cyclone operated at the inlet velocity of 1 m/s showed that the particles having a higher density in the range of 3320 to 3980 kg/m^3 are easier to capture in the container (Figure 8(a)). The results discussed previously (Figures 7(c) and (e)) on the behavior of particles (20 and 100 μm) in the type 2 cyclone operating at 1 m/s are confirmed by the particle distribution shown in Figure 8(b). As can be seen, the larger particles (60 to 100 μm) are densely concentrated at the bottom of the container, while the finer ones are loosely moving at the top of it.

It is interesting to note that the position of the particle in the inlet affects the particle behavior and, therefore, collection efficiency. For example, particles with the same density and size generated at the outer and top walls of the inlet have a greater chance of reaching the container or avoiding the transition over the dotted line in Figure 5, the boundary between upward/downward axial flows and, hence, are more easily captured by the cyclone. However, the effect of particle position in the inlet on the collection efficiency is considered to be less dominant as compared to the particle size and density. These observations correspond to those reported earlier.[23]

C. *Collection Efficiency*

Figures 9(a) and (b) show the contours of collection efficiency for type 1 and type 2 cyclones, respectively, depending on the inlet velocity and the particle size. The contour plots were created using an interpolation technique based on the efficiency obtained for 0.01, 0.1, and 1 m/s. The data on collection efficiency are in line with the results discussed in Section B. The numerically predicted collection efficiency for both types of cyclone generally shows that the cyclone efficiency increases for coarser particles, low inlet velocities, and due to attachment of the container to the bottom of the cyclone. The tendency of decreased efficiency for accelerated flow is also known for molten aluminum filtration through foam filters. Therefore, the depth filtration of aluminum only occurs at very low velocities, namely, typical melt superficial velocities in the range of 0.005 to 0.015 m/s.[24] According to the simulations performed, this velocity range in cyclone application gives the

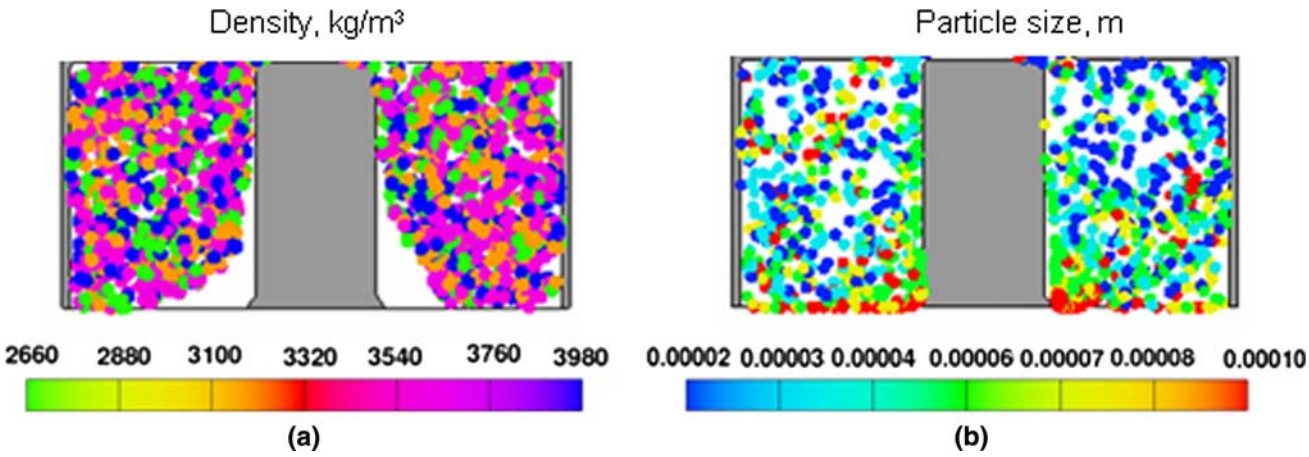

Fig. 8—Particle distribution in the steady state in type 2 cyclone operating at an inlet velocity of 1 m/s with (*a*) different particle densities and identical particle size of 20 μm and (*b*) for different particle sizes and identical particle density of 3300 kg/m^3.

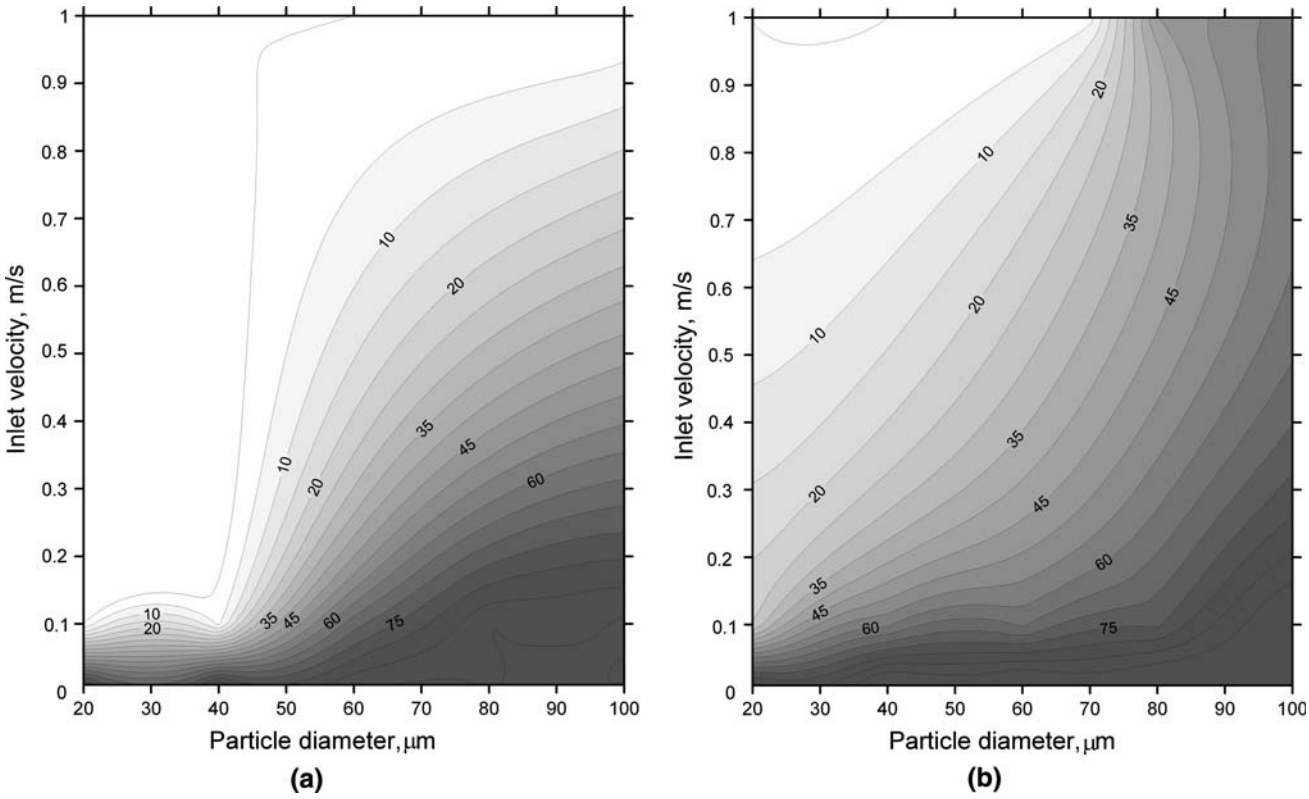

Fig. 9—Collection efficiency of the cyclones according to Table I: (*a*) type 1 and (*b*) type 2, depending on inlet flow velocity and particle diameter. Efficiency is determined as a slope of the function: particle number trapped by the cyclone *vs* time.

collection efficiency of 85 to 95 pct for discrete particles of 20 to 100 μm in size.

By comparing the two types of cyclone, it can be concluded that the collection efficiency at higher inlet velocities (0.2 to 1 m/s) and in the entire particle range can be increased by using the type 2 cyclone. For example, 50 pct efficiency in collection of 100-μm particles can be achieved for this cyclone operating at the inlet velocity as high as 1 m/s, which corresponds to a mass flow rate of 26.6 ton/h.

It is also known that the filter aging, or long-filtration stage, a period following the initial filtration, results in a decreasing efficiency due to accumulation and pick up of particles.[5] Interestingly, the time aspect important for filters can be neglected in cyclone application. For example, the continuous cyclone operation during 24 hours at an inlet velocity of 0.1 m/s and almost 100 pct collection efficiency of 100-μm particles will result in entrapment of approximately $18.5 \cdot 10^6$ particles in the cyclone, which corresponds to a volume of

1227 μm^3. This volume of particles is negligible as compared to the volume of molten aluminum in cyclone. Hence, the cyclone can continue working, maintaining its efficiency.

D. *Flow Control at the Inlet*

At this stage, one can ask how the inflow of the molten aluminum into the cyclone will be controlled during operation and how the pressure will be built up at the inlet. Several calculations are summarized in Figure 10, demonstrating the effect on the inlet velocity and mass flow rate of the metal head in the basin attached to the cyclone inlet. As can be seen, the critical value of the metal head at the inlet is approximately 0.24 m, below which the molten aluminum does not flow through the cyclone. The increase of the metal head up to 0.3 m results in a steep increase of inlet velocity to 0.22 m/s, and then the velocity accelerates proportionally to the metal head at the inlet. To achieve the highest efficiency, it is recommended to maintain the level of the molten aluminum at the inlet as close as possible to the critical value of 0.24 m. Taking into account that the mass flow rate in the range of 10 to 15 ton/h is typical in casting practice and corresponds to the inlet velocity of 0.4 to 0.6 m/s, a series of cyclones can be put in parallel to provide the optimum melt velocity.

VI. SUMMARY

In this article, a numerical simulation technique has been used to evaluate the possibilities of cyclone application in molten aluminum processing by determining the fluid flow for the flow velocities of 0.01, 0.1, and 1 m/s, particle behavior for discrete particle sizes in the range of 20 to 100 μm, and the collection efficiency of the cyclone.

The main conclusion to be drawn from the results of this article is that the cyclone concept seems very promising in application for molten aluminum in a commercially interesting range of inlet velocities and can be used in the separation of impurities commonly present in molten aluminum.

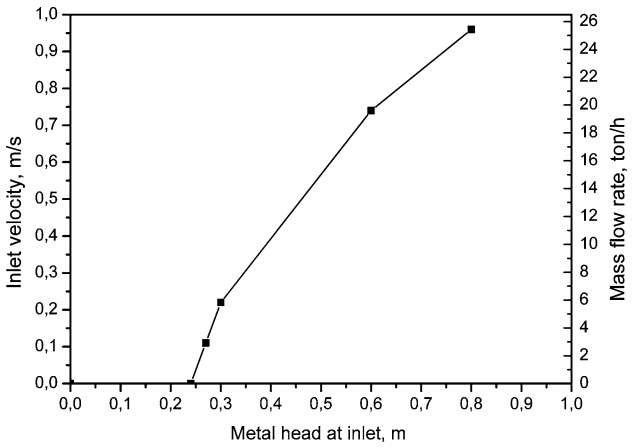

Fig. 10—Effect of metal head at inlet on inlet velocity.

The main concept, the differences and similarities in the design and the operation of the conventional hydrocyclone and the cyclone proposed for impurities removal from molten aluminum are briefly discussed.

The RNG-turbulence model implemented into the commercially available software used in this article has been first validated against experimental and numerical results and then employed for the simulation of the swirl turbulent melt flow in the cyclone. In order to understand the particle behavior in the molten metal, the computation has been performed to quantify the flow and particle trace in the cyclone. The obtained profiles of the axial and tangential velocities were compared and demonstrated a good qualitative agreement with available reference results on hydrocyclones.

Additionally, the effect of the container with the solid core on the flow behavior and collection efficiency was tested. The data on collection efficiency correspond well to the particle behavior in both cyclones for certain flow regimes and particle sizes. It has been shown that the collection efficiency increases for coarser particles and lower inlet velocities. Moreover, the efficiency can be improved by introducing the container with the solid core for retaining captured particles.

Finally, the possibilities of flow control at the inlet and in the cyclone by means of metallostatic pressure in the basin with molten aluminum attached to the inlet were examined. The critical value of 0.24 m was obtained for the specific dimensions of the basin and the cyclone. Therefore, depending on the process conditions of casting in order to achieve higher collection efficiency, it is recommended to keep the level of the molten aluminum as close as possible to the critical value.

While the numerical model can enhance the fundamental understanding of the flow pattern and particle trajectory in the cyclone, a physical experiment is strongly recommended for verification of the existing models, optimum design, and control of cyclones operating with different process conditions.

ACKNOWLEDGMENTS

This work is done within the framework of the research program of the Netherlands Institute for Metals Research (www.nimr.nl), Project MC 4.02134. The authors thank Dr. M. Barkhudarov, Fluid Dynamics Inc., Dr. J. Zuidema, Jr., Corus, and Mr. J. Courtenay, MQP Ltd., for fruitful discussions of the results.

NOMENCLATURE

C_D	drag coefficient
c	coefficient of restitution
$c_{\varepsilon 1}$	coefficient of production in turbulent dissipation transport equation
$c_{\varepsilon 2}$	coefficient of decay in turbulent dissipation transport equation
$c^*_{\varepsilon 2}$	coefficient for RNG model that is function of the shear rate

$c_{\varepsilon 3}$	coefficient of buoyancy in turbulent dissipation transport equation
c_μ	coefficient in turbulent viscosity evaluation
d	diameter (m)
$\mathbf{F}$	overall external forces acting on fluid (N)
G	buoyancy production term
g	acceleration due to gravity (m/s^2)
k	turbulence kinetic energy (m^2/s^2)
p_{in}	inlet pressure (Pa)
p	pressure (Pa)
P	shear production term
Re	fluid Reynolds number
Re_D	particle Reynolds number
S_{ij}	mean strain-rate tensor (s^{-1})
t	time (s)
$\mathbf{u}$	overall velocity vector (m/s)
$\mathbf{u}_p$	particle velocity (m/s)
V_{in}	inlet velocity (m/s)
$\dot{m}$	mass flow rate (kg/s)
x	axis (m)

GREEK SYMBOLS

α_ε	inverse effective Prandtl number for ε
α_k	inverse effective Prandtl number for k
β	constant
ε	turbulence dissipation rate (m^2/s^3)
η_0	constant
μ_{eff}	effective fluid viscosity (kg/m s)
θ	azimutal angle (grad)
μ	molecular fluid viscosity (kg/m s)
μ_t	"eddy" fluid viscosity (kg/m s)
ν	kinematic fluid viscosity
ρ	fluid density (kg/m^3)
τ	stress tensor (N/m^2)

SUBSCRIPTS

i, j	1, 2
p	particle

REFERENCES

1. J. Campbell: *Mater. Sci. Technol.*, 2006, vol. 22, pp. 127–45.
2. C. His, A. Matthews, and J. Braun: *Giesserei*, 1998, vol. 85, pp. 51–54.
3. R. Davis and R.N Dokken: *Proc. 116th TMS Light Metals Annual Meeting*, Denver, CO, Feb. 24–26, 1987, TMS, Warrendale, PA, 1987, pp. 711–16.
4. S. Shivkumar, L. Wang, and D. Apelian: *JOM*, 1991, vol. 43, pp. 26–32.
5. F.A. Acosta G. and A.H. Castillejos E.: *Metall. Mater. Trans. B*, 2000, vol. 31B, pp. 503–14.
6. M.D. Slack and A.E. Wraith: *Proc. Quality in Non-Ferrous Pyrometallurgy*, Vancouver, BC, Aug. 20–24, 1995, Canadian Institute of Mining, Metallurgy and Petroleum, Montreal, PQ, 1995, pp. 227–38. .
7. L. Katgerman and J. Zuidema: *Proc. 134th TMS Light Metals Annual Meeting*, San Francisco, CA, Feb. 13–17, 2005, TMS, Warrendale, PA, 2005, pp. 927–31.
8. Patent Nos. WO2004001078-A1, NL 1020919-C2, and AU2003248155-A1.
9. B. Wang and A.B. Yu: *Miner. Eng.*, 2006, vol. 19, pp. 1022–33.
10. M. Li and R.I.L. Guthrie: *Metall. Mater. Trans. B*, 2000, vol. 31B, pp. 767–77.
11. M. Narasimha, M. Brennan, and P. Holtham: *Int. J. Miner. Process.*, 2006, vol. 80, pp. 1–14.
12. K. Rietema: *Chem. Eng. Sci.*, 1961, vol. 15, pp. 303–09.
13. K. Rietema: *Chem. Eng. Sci.*, 1961, vol. 15, pp. 310–19.
14. *Flow-3D Version 9.2, User's Manual*, 2007 Flow Science Inc., Santa Fe, NM.
15. K.U. Bhaskar, Y.R. Murthy, M.R. Raju, S. Tiwari, J.K. Srivastava, and N. Ramakrishnan: *Miner. Eng.*, 2007, vol. 20, pp. 60–71.
16. V. Yakhot and S.A. Orszag: *J. Sci. Comput.*, 1986, vol. 1, pp. 3–51.
17. B.E. Launder, G.J. Reece, and W. Rodi: *J. Fluid Mech.*, 1975, vol. 68, pp. 537–66.
18. M.S. Slack, R.O. Prasad, A. Bakker, and F. Boysan: *Trans. Inst. Chem. Eng.*, 2000, vol. 78A, pp. 1098–1104.
19. J. Vreeman and F.P. Incropera: *Int. J. Heat Mass Transfer*, 2000, vol. 43, pp. 687–704.
20. X. Cao: *Int. J. Cast. Met. Res.*, 2006, vol. 19, pp. 371–74.
21. L. Zhang: *Proc. 134th TMS Annual Meeting: Characterization of Minerals Meals. and Materials*, Orlando, FL, Feb. 25–Mar. 1, 2007, TMS, Warrendale, PA, 2007, pp. 35–45.
22. A. Gupta and R. Kumar: *Int. J. Heat Fluid Flow*, 2007, vol. 28, pp. 249–61.
23. L. Ma, D.B. Ingham, and X. Wen: *J. Aerosol Sci.*, 2000, vol. 31, pp. 1097–119.
24. L.S. Aubrey and J.E. Dore: *Proc. 122nd TMS Light Metals Annual Meeting*, Denver, CO, Feb. 21–25, 1993, TMS, Warrendale, PA, 1993, pp. 1009–20.